Arrested coalescence of viscoelastic droplets with internal microstructure

Amar B. Pawar,[ab] Marco Caggioni,[a] Richard W. Hartel[b] and Patrick T. Spicer*[a]

Received 18th February 2012, Accepted 24th April 2012
DOI: 10.1039/c2fd20029e

There are many new approaches to designing complex anisotropic colloids, often using droplets as templates. However, droplets themselves can be designed to form anisotropic shapes without any external templates. One approach is to arrest binary droplet coalescence at an intermediate stage before a spherical shape is formed. Further shape relaxation of such anisotropic, arrested structures is retarded by droplet elasticity, either interfacial or internal. In this article we study coalescence of structured droplets, containing a network of anisotropic colloids, whose internal elasticity provides a resistance to full shape relaxation and interfacial energy minimization during coalescence. Precise tuning of droplet elasticity arrests coalescence at different stages and leads to various anisotropic shapes, ranging from doublets to ellipsoids. A simple model balancing interfacial and elastic energy is used to explain experimentally observed coalescence arrest in viscoelastic droplets. During coalescence of structured droplets the interfacial energy is continuously reduced while the elastic energy is increased by compression of the internal structure and, when the two processes balance one another, coalescence is arrested. Experimentally we observe that if either interfacial energy or elasticity dominates, total coalescence or total stability of droplets results. The stabilization mechanism is directly analogous to that in a Pickering emulsion, though here the resistance to coalescence is provided *via* an internal volume-based, rather than surface, structure. This study provides guidelines for designing anisotropic droplets by arrested coalescence but also explains some observations of "partial" coalescence observed in commercial foods like ice cream and whipped cream.

1 Introduction

Coalescence is a process of merging two or more droplets into a single, usually spherical, droplet. The driving force for coalescence to proceed, once initiated, is the reduction in interfacial energy by a minimization of the surface-to-volume ratio. Coalescence is a common instability mechanism in emulsions and its initiation is often sterically opposed by the addition of species like surfactants and polymers that adsorb to droplet surfaces.[1–4] Adsorbed colloids can also prevent coalescence initiation in Pickering emulsions[5–7] by forming a sufficiently continuous surface layer on droplets that provides steric stabilization. While stabilizing emulsions against the initiation of coalescence is a common goal, coalescence can also be initiated but then halted before formation of a single spherical droplet, a phenomenon known as

[a]*Complex Fluid Microstructures, Corporate Engineering, Procter and Gamble Co., 8256 Union Center Blvd., West Chester, Ohio, USA. E-mail: spicer.pt@pg.com*
[b]*Department of Food Science, University of Wisconsin Madison, 105 Babcock Hall, 1605 Linden Drive, Madison, WI, USA*

arrested coalescence.[8–13] Although arrested coalescence in food processes has been widely studied,[14–17] the exact mechanisms of resistance to coalescence and the stabilization of arrested structures are not yet fully understood because they typically occur in complex systems that do not permit the isolation of key phenomena.[8,9,18,19]

More fundamental studies [11,20] have shown that arrested structures require a dynamic balance between the forces driving shape relaxation and an opposing force. Coalescence can be stably arrested by droplet elasticity at the droplet surface[14] or within its volume.[21] While coalescence arrested by interfacial elasticity has led to fabrication of novel materials such as bijels[22,23] and armored droplets,[24,25] volume elasticity is often crucial for fabrication of structured food emulsions such as ice cream and whipped cream.[9,18,21] Through similar, but more complex, mechanisms non-spherical biological shapes can be formed by bacteria and viruses during dynamic processes like cell division and protrusion.[26] Recent work has also created simple cell analogues with emulsion drops containing elastic networks of actin.[27]

Arrest at flat interfaces [28,29] and on the surface of liquid doublets has only recently been studied for model systems.[20,30] Pawar *et al.*[20] found that the elasticity of the droplet surface determined the degree of arrest and, thus, the shape of the resultant liquid doublets or ellipsoids. In addition to surface structures, the elasticity of an entire droplet volume can also arrest coalescence to form novel colloidal structures but such effects have not been studied in model systems. In this article we make *in situ* observations of coalescing model viscoelastic droplets to isolate contributions of interfacial tension and elasticity to arrest. When elastic and interfacial forces possess similar magnitude, stable arrested droplet structures are found, while if either elastic or interfacial forces dominate then total stability or total coalescence, respectively, is observed.

2 Experimental details

Partially crystalline oil droplets are prepared by making oil-in-water (O/W) emulsions using oil containing anisotropic wax crystals.[10] The emulsions are then diluted to study droplet coalescence behavior by micromanipulation.

2.1 Emulsion preparation and characterization

Emulsions are prepared by mixing equal volumes (5 ml each) of an oil and aqueous phase. The dispersed oil phase consists of a mixture of hexadecane (99%, Sigma Aldrich) and wax (Petrolatum, Unilever) while the continuous aqueous phase consists of a 0.5 wt% microfibrous cellulose (MFC, CP-Kelco) dispersion ($\sigma_y \sim 0.17$ Pa) and 10 mM sodium dodecyl sulfate (SDS) (99%, Fluka) surfactant solution. The small yield stress of the continuous phase avoids sedimentation and uncontrolled movement of the small droplets during manipulation. The emulsion is made by combining the oil and the aqueous phases, heating to 75 °C, then shaking by hand for 10 s. The dispersed phase is initially a homogeneous solution but, as the emulsion cools down to room temperature, wax (mp $\sim$ 40–60 °C) crystallizes inside the droplets. The hexadecane completely wets the crystals, containing them within the emulsion drop volume. The wax crystals are anisotropic solids with an aspect ratio $\sim$10, as seen in Fig. 1, and are weakly attractive as gelation of the wax crystals is sometimes observed within droplets. The elastic modulus (G') of the wax–oil dispersion is measured in the linear viscoelastic regime by oscillatory shear experiments (AR 2000) at a strain of 0.1%.

Emulsions are fabricated to produce partially crystalline droplets with variable solid content (10%–50%). Emulsions are further diluted $\sim$10$\times$ with an MFC dispersion without surfactant for the micromanipulation experiments.

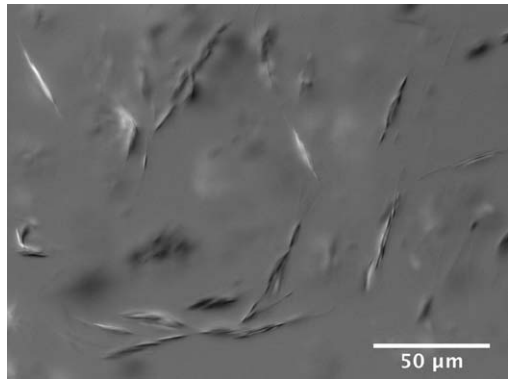

Fig. 1 Dispersion of anisotropic wax crystals in hexadecane (~20% w/w wax).

2.2 Droplet coalescence study

Coalescence of two partially crystalline droplets is induced and observed *in situ* by micromanipulation experiments.[31–33] One of the droplets is held at the tip of a pre-pulled capillary by applying suction and is then manually contacted with the other droplet to study their coalescence behavior.

Tapered capillaries are fashioned from standard borosilicate glass capillaries (1 mm OD and 0.5 mm ID, Sutter Instruments) with a Micropipette Puller (Model P-97; Sutter Instruments). The tip of a pulled capillary is flattened using a Microforge (Model MF-830; Narishige Int'l. USA). The other end of the capillary is connected to a water reservoir (10 ml open syringe) by rubber tubing. Changing the height of the water reservoir adjusts the hydrostatic pressure applied at the flattened tip of the capillary, enabling manipulation of droplets. The capillary is mounted on a 3-axis coarse manipulator (Narishige Int'l USA) which is attached to a microscope stage (Zeiss axioplan-2). A diluted drop of emulsion (~1 ml) is placed on a glass slide and the tip of the mounted capillary is aligned with one of the partially crystalline droplets using the micromanipulator. The droplet is drawn toward the capillary tip by applying suction (negative hydrostatic pressure). Applied suction is adjusted such that it holds the droplet stationary at the tip of the capillary without squeezing out any oil. The captured droplet is aligned and manually contacted with a second partially crystalline droplet suspended in the continuous phase and their coalescence is observed. Microscopic observation of coalesced droplets after 15 min is used to differentiate between total coalescence, arrested coalescence, and total stability behavior.

3 Results and discussion

As two droplets contact, coalescence is initiated when a liquid neck forms between them. The drops are then pulled together into a single spherical drop *via* flow of oil through the liquid neck. During the coalescence process, the instantaneous deformation of the shape is a function of the emulsion interfacial forces, as described by the Laplace pressure,[34] $P \propto \gamma/R$, where γ is the oil–water interfacial tension and R is droplet radius. The resulting change in shape of the coalescing structure is then a function of the instantaneous strain:

$$\varepsilon = \frac{\Delta L}{L_0} \tag{1}$$

where L_0 is the initial length before coalescence is initiated, $L_0 = 4 \times R$, and ΔL is the linear deformation. Fig. 2 illustrates coalescence of two hexadecane drops

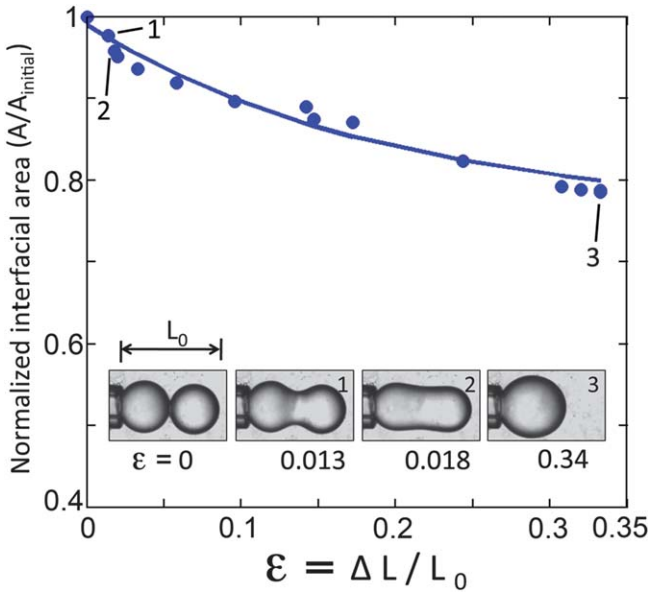

Fig. 2 Change in interfacial area as a function of strain during coalescence of hexadecane drops. Micrographs 1–3 show coalescing droplets at intermediate stages corresponding to the points labeled above.

without wax crystals and plots the change in interfacial area with strain. For coalescence of the drops in Fig. 2 only the drop viscosity resists the Laplace pressure-driven oil flow. The neck radius grows with coalescence and eventually interfacial tension drives the drop into a spherical shape.[35] As coalescence progresses , the interfacial area continuously decreases while ΔL, and thus the strain, increases accordingly. A reduction to ~79%, or $2^{-1/3}$, of the original interfacial area is achieved during total coalescence, corresponding to a strain of ~0.37, or $1–2^{-2/3}$, for identical drops.

Evolution of coalescing shapes thus depends on interfacial tension and the continuous and dispersed phase rheology. Fig. 2 indicates that the interfacial area decays exponentially with strain and can be fit using:

$$A = A_0 + A_1 \exp\left(-\frac{\varepsilon}{A_2}\right) \tag{2}$$

where $A_0 = 0.76$, $A_1 = 0.23$, and $A_2 = 0.19$ correspond to the data in Fig. 2. Coalescing structures progress through various non-spherical shapes in Fig. 2 before reaching a final spherical one. Arresting coalescence at any of these intermediate shapes, and thus strains, is possible if the droplets offer enough elastic resistance to balance the Laplace pressure gradient.[20]

In contrast to our earlier study of interfacial elasticity-driven arrested coalescence, here we study coalescence of droplets whose interior volumes are elastic as a result of varying solid content. Fig. 3 reports the elastic modulus of wax–hexadecane dispersions for several solid levels. The partially crystalline oil phase elastic modulus grows as a power law with exponent ~4.8 with increasing solid content and, similar to our earlier findings for Pickering emulsions, we expect coalescence to be arrested at different stages depending on these parameters.

The coalescence behavior of partially crystalline droplets with increasing solid content is illustrated in Fig. 4. Fig. 4 a.1–e.1 indicate two partially crystalline droplets before coalescence is initiated with $\phi = 0.15$, 0.30, 0.40, 0.45, and 0.50 solid

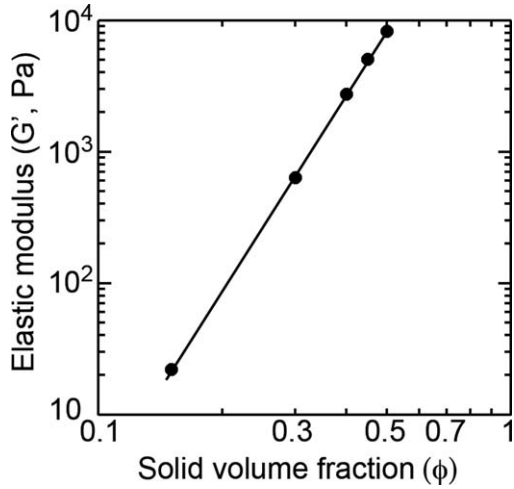

Fig. 3 Elastic modulus of wax–hexadecane dispersion as the volume fraction of wax is varied.

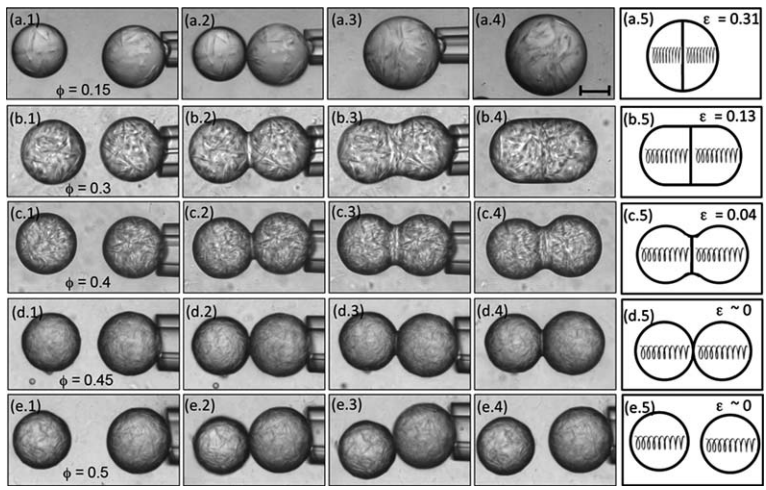

Fig. 4 Micrographs showing coalescence behavior of viscoelastic droplets, left to right, as the solid volume fraction is increased from top to bottom. Also shown are schematics of the final strain of each droplet pair. Scale bar = 50 μm.

volume fraction, respectively. As droplets are contacted coalescence begins and liquid oil flows from droplets to the coalescing neck (Fig. 4 a.2–d.2). At low solids fractions, around $\phi = 0.15$, droplets behave like weak gels that deform easily because of their low elastic moduli (Fig. 3). As a result, during coalescence the interfacial energy dominates elastic energy and the drop completely relaxes into a final spherical shape (Fig. 4 a.4). As the solids fraction is increased, the droplet elastic modulus increases and for $\phi = 0.30$–0.45 the particle network elasticity balances the Laplace driving force at an intermediate shape and arrested coalescence occurs (Fig. 4 b.4–d.4). It is clear that increasing the droplet elasticity arrests coalescence at earlier stages, changing the resulting shape. Further increasing solids fraction to $\phi = 0.50$ raises the droplet elasticity enough to completely prevent coalescence initiation (Fig. 4 e.4), at least to the limits of our observations. The progression of shapes and arrest in Fig. 4 is similar to our results for Pickering droplets[20] and the

stabilization at high solids fractions is directly analogous to the interfacially-based stabilization seen in Pickering emulsions.[7]

Clearly the formation of stable arrested doublets results from a balance of the interfacial driving force and the elastic reaction force of the droplet microstructure. The partially crystalline droplets studied here contain an elastic network of solid crystals saturated with liquid oil: a poroelastic colloidal gel. During coalescence, Laplace pressure gradients exert stress on and deform the solid network. As coalescence progresses the drop area and, thus, the interfacial energy, $E_{\text{interfacial}}$, is continuously reduced:

$$E_{\text{interfacial}} = A\gamma \tag{3}$$

where γ is 10 mN m^{-1}, and A is the total interfacial area of two coalescing droplets. While coalescence decreases interfacial energy, the deformation or strain of the elastic droplet microstructure leads to an increase of elastic energy, E_{elastic}, stored within the microstructure:

$$E_{\text{elastic}} = \frac{3}{2} G' \varepsilon^2 V \tag{4}$$

where G' is the droplet shear modulus that has been multiplied by three to yield the Young's modulus [36] and V is total volume of the coalescing droplets. The decreasing interfacial energy, eqn (3), and increasing elastic energy, eqn (4), can be balanced at any strain in the range between total stability, $\varepsilon = 0$, and total coalescence, $\varepsilon = 0.37$, stabilizing doublet shapes at various minimum energy states. A simple energy balance can be used to explore the minima corresponding to stable arrested coalescence states.

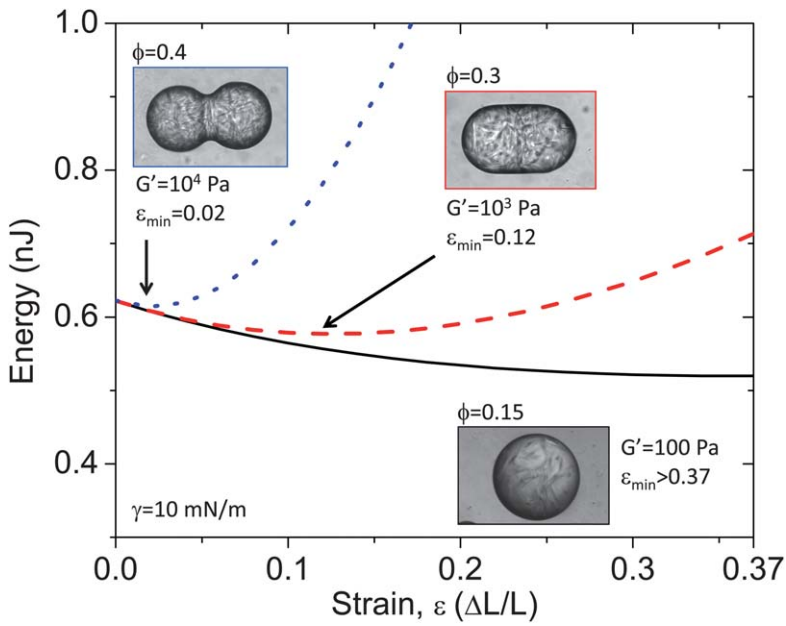

Fig. 5 Comparison of change in total energy during arrested and total coalescence of droplets. A zero strain corresponds to droplets before coalescence and a maximum strain of 0.37 represents total coalescence into a spherical droplet. The two arrows indicate the location of energy minima for each of the arrested coalescence cases.

We calculate the change in energy during coalescence of droplets with three relevant elastic moduli, $G' = 100$ Pa, 10^3 Pa, and 10^4 Pa, and plot the total energy against droplet deformation in Fig. 5. Here we assume the interfacial energy is solely a function of interfacial area during coalescence, that the droplet elastic modulus is a constant with strain, and that the shape evolution in Fig. 2 approximates the behavior of partially crystalline droplets. We also neglect any minimum deformation required to overcome disjoining pressures and initiate coalescence.[37,38] Accordingly, the interfacial area decays exponentially with strain (eqn (2)). However, the elastic energy (eqn (4)) varies as a power law with strain and is proportional to the elastic modulus. Combining both energy terms, a minimum in the total energy occurs when the stored elastic energy increases to attain the same magnitude as the interfacial energy lost by drop compression during coalescence.

In Fig. 5 for droplets with low elastic modulus, $G' = 100$ Pa, the bottom solid curve indicates the change in elastic energy is negligible *versus* the change in interfacial energy. As a result, the total energy is dominated by the exponential decay of interfacial energy and relaxes to a minimum value at a strain corresponding to a single sphere, $\varepsilon = 0.37$. For an intermediate elastic modulus of $G' = 10^3$ Pa the middle dashed curve in Fig. 5 has a minimum at an intermediate $\varepsilon = 0.12$, approximating that of the non-spherical shape shown. Further increasing the droplet elastic modulus increases the rate of elastic energy storage during coalescence and enables arrest at much smaller strains, moving the minimum down to $\varepsilon = 0.02$ in the top dotted curve of Fig. 5 and qualitatively matching the results in Fig. 4.

While this simple model correctly captures the mechanism underlying the arrested coalescence state, it is not complete. For example, our model predicts a minimum in the total energy, even at high values of G' and at vanishingly low strains, though experimentally we see no coalescence initiation for such high modulus structures. This discrepancy could arise because the model does not include coalescence initiation even though experimentally our drops required a minimum critical strain, $\varepsilon_{\text{critical}} \sim 0.01$, to trigger coalescence. A more detailed model quantifying the condition for coalescence onset appears necessary to fully describe an elastic stabilization mechanism but the model provides a starting point for understanding arrested coalescence and for mapping the expected behavior of droplets in practical food processes.

Using the above conceptual model, we predict that total coalescence and arrested coalescence can be obtained by appropriately tuning the droplet elastic modulus and interfacial tension. Adding eqn (3) and eqn (4) to obtain the total energy of two coalescing droplets, taking the derivative with respect to strain, then equating the result to zero allows us to locate minima for a range of curves like those plotted in Fig. 5:

$$\gamma = \frac{A_2}{A_1}\exp\left(\frac{\varepsilon_{\min}}{A_2}\right) G' R\varepsilon_{\min} \tag{5}$$

We can use eqn (5) to calculate, for a droplet of radius R, the elastic moduli and interfacial tensions yielding either coalesced or arrested structures and we can speculate on the existence of a region of elastic stabilization as well. Plotting lines of constant minimum strain in Fig. 6 for the limiting cases of complete coalescence, $\varepsilon_{\min} = 0.37$, and total stability against coalescence, $\varepsilon_{\min} = \varepsilon_{\text{critical}} \sim 0.01$, produces a map of the three regions for identical size elastic droplets of a given radius. The left region corresponds to the states of complete relaxation to a spherical shape and is separated from the middle arrested coalescence region by the $\varepsilon_{\min} = 0.37$ line. The right region represents the states where we experimentally observe total stability against coalescence and is bounded on its left side by the dashed $\varepsilon_{\min} = 0.01$ line. Within the arrested coalescence region the structures can vary from ellipsoidal to doublet shapes. If further validated, such a map could provide a useful design basis for emulsion formulation and processing depending on the desired microstructure and bulk rheology of a product. Ultimately more experiments are

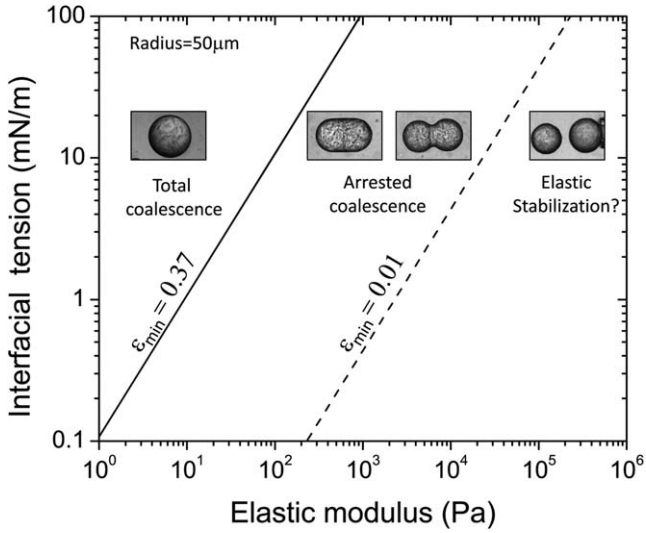

Fig. 6 Coalescence behavior map for identical size 50 μm droplets showing a conceptual basis for designing droplet structures using physical properties like interfacial tension and droplet elasticity.

required to test these ideas given the very basic nature of the proposed model, but its consistency with our experimental data is encouraging.

Here, as in the case of Pickering emulsions,[20] arrested coalescence occurs as the result of a balance between interfacial and elastic forces. By moving the arresting elastic microstructure from the drop surface to its volume, we change the mechanism of arrest from a jamming due to increased volume fraction to a reaction due to elastic deformation. While for Pickering droplets the solids surface concentration increases during coalescence, the solids volume fraction in the drops examined here remains constant. Thus the arrest is not due to irreversible jamming but to a reversible elastic reaction. The distinction is important as a completely jammed interface, like those seen in armored droplets [24] and other arrested Pickering emulsions, [20] usually will not permit subsequent addition of droplets to form a larger network. However, partially crystalline droplets can form unique supracolloidal materials with multi-unit structures *via* sequential arrested coalescence, as shown in Fig. 7. Furthermore, in certain food emulsions like ice cream and whipped

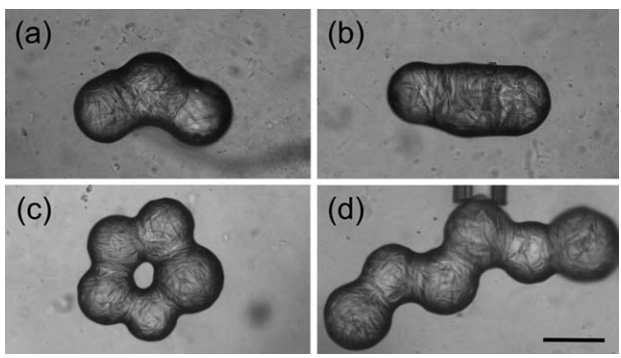

Fig. 7 Anisotropic structures of partially crystalline shapes fabricated by arrested coalescence of three or more droplets. Scale bar = 100 μm.

toppings, volume-spanning rheological networks of clustered fat droplets are formed during processing, providing structure and influencing physical and sensorial properties.[17] Our study may provide a means to design and characterize such applied systems using commonly measured parameters.

Acknowledgements

We gratefully acknowledge discussions of these results with Eric Furst (U. Delaware), Steven Hudson (NIST), and Véronique Trappe (U. Fribourg). We also sincerely thank an anonymous referee for valuable commentary on the manuscript.

References

1 F. Leal-Calderon, V. Schmitt and J. Bibette, *Emulsion Science: Basic principles*, Springer, 2007.
2 K. S. Birdi, *Surface and colloid chemistry: Principles and applications*, CRC Press Taylor and Francis group, 2010.
3 P. C. Hiemenz and R. Rajagopalan, *Principles of Colloid and Surface Chemistry*, Marcel Dekker, Inc., 1997.
4 B. P. Binks, *Modern Aspects of Emulsion Science*, The Royal Society of Chemistry, 1998.
5 S. U. Pickering, *J. Chem. Soc. Trans.*, 1907, **91**, 2001–2021.
6 N. D. Denkov, I. B. Ivanov, P. A. Kralchevsky and D. T. Wasan, *J. Colloid Interface Sci.*, 1992, **150**, 589–593.
7 B. P. Binks, *Curr. Opin. Colloid Interface Sci.*, 2002, **7**, 21–41.
8 E. Fredrick, P. Walstra and K. Dewettinck, *Adv. Colloid Interface Sci.*, 2010, **153**, 30–42.
9 P. Walstra, *Physical Chemistry of Foods*, Marcel Dekker Inc., 2003.
10 J. Giermanska, F. Thivilliers, R. Backov, V. Schmitt, N. Drelon and F. Leal-Calderon, *Langmuir*, 2007, **23**, 4792–4799.
11 A. R. Studart, H. C. Shum and D. A. Weitz, *J. Phys. Chem. B*, 2009, **113**, 3914–3919.
12 A. B. Subramaniam, M. Abkarian and H. A. Stone, *Nat. Mater.*, 2005, **4**, 553–556.
13 J. Giermanska-Kahn, V. Laine, S. Arditty, V. Schmitt and F. Leal-Calderon, *Langmuir*, 2005, **21**, 4316–4323.
14 K. Boode, P. Walstra and A. E. A. de Groot-Mostert, *Colloids Surf., A*, 1993, **81**, 139–151.
15 K. Boode and P. Walstra, *Colloids Surf., A*, 1993, **81**, 121–137.
16 D. Rousseau, *Food Res. Int.*, 2000, **33**, 3–14.
17 F. Thivilliers-Arvis, E. Laurichesse, V. Schmitt and F. Leal-Calderon, *Langmuir*, 2010, **26**, 16782–16790.
18 H. D. Goff, *J. Dairy Sci.*, 1997, **80**, 2620–2630.
19 J. Benjamins, M. H. Vingerhoeds, F. D. Zoet, E. de Hoog and G. A. van Aken, *Food Hydrocolloids*, 2009, **23**, 102–115.
20 A. B. Pawar, M. Caggioni, R. Ergun, R. W. Hartel and P. T. Spicer, *Soft Matter*, 2011, **7**, 7710–7716.
21 F. Leal-Calderon, F. Thivilliers and V. Schmitt, *Curr. Opin. Colloid Interface Sci.*, 2007, **12**, 206–212.
22 E. M. Herzig, K. A. White, A. B. Schofield, W. C. K. Poon and P. S. Clegg, *Nat. Mater.*, 2007, **6**, 966–971.
23 F. Thivilliers, N. Drelon, V. Schmitt and F. Leal-Calderon, *Europhys. Lett.*, 2006, **76**, 332–338.
24 A. B. Subramaniam, M. Abkarian, L. Mahadevan and H. A. Stone, *Nature*, 2005, **438**, 930–930.
25 A. B. Subramaniam, M. Abkarian, L. Mahadevan and H. A. Stone, *Langmuir*, 2006, **22**, 10204–10208.
26 T. J. Mitchison, G. T. Charras and L. Mahadevan, *Semin. Cell Dev. Biol.*, 2008, **19**, 215–223.
27 M. Claessens, R. Tharmann, K. Kroy and A. Bausch, *Nat. Phys.*, 2006, **2**, 186–189.
28 H. Xu, S. Melle, K. Golemanov and G. Fuller, *Langmuir*, 2005, **21**, 10016–10020.
29 B. Madivala, S. Vandebril, J. Fransaer and J. Vermant, *Soft Matter*, 2009, **5**, 1717–1727.
30 H. L. Cheng and S. S. Velankar, *Langmuir*, 2009, **25**, 4412–4420.
31 E. A. Evans and R. Skalak, *Mechanics and Thermodynamics of Biomembranes*, CRC Press, 1980.
32 R. Kwok and E. Evans, *Biophys. J.*, 1981, **35**, 637–652.
33 S. Lee, D. H. Kim and D. Needham, *Langmuir*, 2001, **14**, 5537–5543.

34 H. J. Butt, K. Graf and M. Kappl, *Physics and Chemistry of Interfaces*, Wiley VCH GmbH and Co. KGaA, 2003.
35 M. Wu, T. Cubaud and C. M. Ho, *Phys. Fluids*, 2004, **16**, L51–L54.
36 M. A. Biot, *J. Appl. Phys.*, 1941, **12**, 155–164.
37 J. Bibette, D. Morse, T. Witten and D. Weitz, *Phys. Rev. Lett.*, 1992, **69**, 2439–2442.
38 D. Filip, V. Uricanu, M. Duits, W. Agterof and J. Mellema, *Langmuir*, 2005, **21**, 115–126.

